Extracting Pavement Surface Distress Conditions Based on High Spatial Resolution Multispectral Digital Aerial Photography

Su Zhang, Susan M. Bogus, Christopher D. Lippitt, Paul R.H. Neville, Guohui Zhang, Cong Chen, and Vanessa Valentin

Abstract

State transportation agencies regularly collect data on pavement surface distresses. These data are used to assess overall pavement conditions and to make maintenance and repair decisions. Routinely-acquired and publically-available high spatial resolution (HSR) multispectral digital aerial photography provides a potential method for collecting distress information that can supplement or replace currently-used technologies. Principal component analysis and linear least squares regression models were used to evaluate the potential of using HSR multispectral digital aerial photographs to estimate pavement surface overall distress conditions. Various models were developed using HSR multispectral digital aerial photographs of different spatial resolution (6-inch, 12-inch, and 24-inch) and reference pavement surface distress data collected manually at multiple sample sites using standard protocols. The results show that the spectral response of HSR multispectral digital aerial photographs correlate strongly with reference distress rates at all tested spatial resolutions, but the 6-inch aerial photos exhibit the strongest correlation ($R^2 > 0.95$), even when using only half of the sample sites ($R^2 > 0.92$). These results indicate that straightforward analysis of HSR multispectral digital aerial photographs, routinely acquired by most municipalities and states, can permit assessment of pavement surface distress conditions as well as current manual evaluation protocols.

Introduction

The serviceability of road networks primarily relies on pavement conditions, and subsequently, federal, state, and local transportation agencies dedicate a large amount of time and money to routinely evaluate pavement conditions as part of their management programs. Pavement surface distress data are collected and used by these agencies to determine the serviceability of individual roads, and then to make decisions on the distribution of limited resources for maintenance and construction projects.

Currently, most state and local transportation agencies use either manual evaluation or automated evaluation to collect data solely for the purpose of pavement surface evaluation at significant expense (McGhee, 2004). We therefore explore the utility of routinely-acquired and publically-available high spatial resolution (HSR) visible range digital aerial photography to supplement or replace dedicated surveys of pavement surface condition. Many counties and municipalities routinely acquire HSR multispectral digital aerial photos, and most make these images freely available to the public. These photos cover all ground features including roadways, meaning they contain information that may permit discrimination of pavement surface distress. Modern aerial photographs are in digital format, which means they can be readily shared with partner agencies and analyzed to produce standardized results through image processing techniques. The availability of these images offers the potential of using routinely-collected and publically-available data for standardized evaluation of pavement surface distress, reducing the evaluation cost and time while improving the comparability of results.

This paper explores the utility of routinely-acquired and publically-available HSR multispectral digital aerial photography for the evaluation of overall pavement surface distress. Specifically, the intent of this study is to examine how well overall pavement surface distress can be estimated from HSR multispectral digital aerial photography. Principal components analysis (PCA) and linear least squares regression models were used to evaluate the potential of using HSR multispectral digital aerial photographs to infer pavement surface distress.

Background

Pavement surface distress information is essential to pavement management. Pavement management activities and decisions at all levels (i.e., federal, state, and local) are supported by pavement surface condition information of varying detail (Haas *et al.,* 1994). Pavement evaluation can lead to effective allocation of limited resources for timely maintenance and repair (Haas *et al.,* 1994; Hudson and Uddin, 1987). Pavement evaluation is also necessary to measure the effectiveness of various maintenance techniques and repair methods (Hudson *et al.,* 1987; Hudson and Uddin, 1987).

To characterize the conditions of existing pavements, surveys are conducted to assess one or more of four criteria: roughness, distress, structural capacity, and friction (Gramling, 1994). Pavement distress and roughness are the basic elements typically included in quantification of the overall pavement condition, although structural capacity and friction may also be incorporated (Gramling, 1994; Prakash *et al.,* 1994).

Current Pavement Surface Distress Evaluation Methods

Currently, two types of pavement surface distress evaluation methods have been broadly adopted by state and local

Su Zhang, Susan M. Bogus, Guohui Zhang, Cong Chen, and Vanessa Valentin are with the Department of Civil Engineering, University of New Mexico, Albuquerque, NM 87131-0001 (suzhang@unm.edu).

Christopher D. Lippitt is with the Department of Geography and Environmental Studies, University of New Mexico, Albuquerque, NM 87131-0001.

Paul R.H. Neville is with the Earth Data Analysis Center, University of New Mexico, Albuquerque, NM 87131-0001.

Photogrammetric Engineering & Remote Sensing
Vol. 81, No. 9, September 2015, pp. 709–720.
0099-1112/15/709–720

doi: 10.14358/PERS.81.9.709

transportation agencies: automated evaluation (machine observation and machine analysis) and manual evaluation (human observation and human analysis). Most state or local transportation agencies use one of these two aforementioned methods or a combination of them. Each method has advantages and disadvantages.

Only a few state and local transportation agencies are still using manual methods to survey the surface distress of highway pavement (Bandini *et al.,* 2012). Using this method, data are collected by inspectors walking along a section of pavement and rating the level of distress. These data are primarily handwritten data and attached to archived images acquired by inspectors on the ground. Manual evaluation methods can collect detailed information for various types of distresses, and it is the reason that this method is still used. However, this method is expensive, extremely labor intensive, time-consuming, and data collected by different inspectors can exhibit a high degree of variability (Bogus *et al.,* 2010). Manual evaluation is, therefore, sometimes unable to provide meaningful quantitative information, and eventually leads to inconsistencies in distress conditions over space and across evaluation (Cheng *et al.,* 1999; Hudson and Uddin, 1987; Wang and Li, 1999; Wang, 2000). In addition, manual evaluation relies on the subjective evaluation of distress type, extent, and severity by a trained inspector based on visual observation (Hudson and Uddin, 1987), which means the evaluation results are prone to subjective bias. Another problem with manual evaluation is that it is potentially dangerous to inspectors. Crews must walk along the side the road to perform their evaluation and, despite safety precautions (e.g., safety training and high-visibility garments), are exposed to significant risk of personal injury.

In an attempt to address the shortcomings of manual evaluation, many transportation agencies have adopted automated technology to conduct distress surveys (Bandini *et al.,* 2012). The automated methods typically include the use of vehicle-mounted electronic sensors at a fine enough spatial resolution to detect individual distress measures (e.g., cracks) in the pavement surface. The application of automated surveys based on a variety of electronic sensors (e.g., video cameras and laser sensors) became common in the 1980s (Curphey *et al.,* 1985; Haas *et al.,* 1985; Hudson and Uddin, 1987). These various types of sensors are designed to detect and assess either a specific type of individual distress such as transverse cracks or a specific type of pavement such as concrete (Uddin *et al.,* 1987; Hudson *et al.,* 1987; Hudson and Uddin, 1987; Mahler *et al.,* 1991; Georgopoulos *et al.,* 1995; Pynn *et al.,* 1999; Lee and Kim, 2005; Huang and Xu, 2006; Zhou *et al.,* 2006; Oliveira and Correia, 2008; Nguyen *et al.,* 2009; Coudray *et al.,* 2010; Gavilan *et al.,* 2011; Koch and Brilakis, 2011; Adarkwa and Attoh-Okine, 2013).

Although automated evaluations can collect detailed information quickly and safely, and technological advances in computer hardware and imaging recognition have improved the performance of the automated evaluation methods, serious problems still remain in the areas of implementation costs, processing speed, and accuracy (Wang, 2000). Automated methods require significant time to process data to extract useful information, since it requires very complicated analytical models and algorithms (Wang, 2000). These methods require substantial technical expertise and are expensive to deploy, requiring specially trained operators. In addition, data are collected on the ground as a single task and cannot be shared with other partner agencies to reduce the cost because a single image can only cover a small area which is usually less than five square meters (McGhee, 2004). For example, the Vermont Agency of Transportation reported costs of up to $170 USD per mile in urban areas for automated evaluation (McGhee, 2004).

Pavement Surface Distress Evaluation from Aerial Photography

Pavement evaluation from aerial photography is not a new idea, but is also not used for operational evaluation of pavement surface distresses yet. The application of an aerial photography-based evaluation method to pavement surface distress was first implemented in the 1950s. Several studies (McMaster and Legault, 1952; Stoeckeler, 1968; Stoeckeler, 1970) focused on visually comparing analog panchromatic aerial photographs to determine pavement surface distress. They concluded that untreated cracks and other pavement defects (e.g., patching and bleeding) can be identified through the visual analysis. Although they concluded that visual analysis of panchromatic analog aerial photography is a practical means of conducting pavement condition surveys, it is not used for operational pavement surface distress evaluation. This is because cracks are distinguishable only in large scale (e.g., 1:100) analog panchromatic aerial photographs and the associated cost is extremely high.

Chen *et al.* (2011) proposed a method of analyzing very high spatial resolution (VHSR) multispectral digital aerial photography to detect large cracks on bridge pavement. Crack type, length, width, and severity were measured from the post-processed VHSR multispectral digital aerial photography, and then these measurement results were used in a bridge surface condition index (BSCI) rating system to calculate the distress conditions. However, in their research, the collection of the VHSR multispectral digital aerial photography was customized to fulfill the specific bridge pavement evaluation purpose. In other words, the collected aerial photos, like the pavement evaluation methods that are currently used operationally, serve only a single purpose and therefore represent an expensive option for routine distress evaluation.

There are many programs to routinely collect HSR multispectral digital aerial photography. For example, with the support of the National Agricultural Imagery Program (NAIP), the United States Geological Survey (USGS) and the United States Department of Agriculture (USDA) regularly acquire digital, color-infrared, ortho-corrected aerial photography which covers all states at 1-meter spatial resolution, and they provide the data to the public for free. Many counties and cities now routinely acquire natural color 6-inch (0.1524-meter) and even 3-inch (0.0762-meter) spatial resolution, ortho-corrected aerial photos. In addition, some states have initiated the program to regularly acquire statewide aerial photos. For example, the State of Missouri images the entire state regularly with 2-foot (0.6096-meter) spatial resolution multispectral digital aerial photographs (Wright, 2014). It would not be hard to imagine more states to moving to do so because the uses for these data continue to expand.

Past and current research for pavement distress evaluation has focused on the detection of individual distresses (e.g., an individual crack). This information is commonly aggregated to determine the overall level of pavement distress, which is then used by transportation agencies for planning purposes. According to Stoeckeler (1970), cracks are only distinguishable in large-scale (e.g., 1:100) aerial photographs. A key limitation of the routinely collected HSR multispectral aerial photography is that its spatial resolution is too coarse to enable the detection and quantification of individual distresses. As a result, this research does not focus on assessing individual distresses, but rather, on estimating the overall condition by analyzing the brightness and variation of resolution cells. Specifically, the research presented here is focused on analyzing HSR multispectral digital aerial photographs to determine overall pavement distress rates through pixel-based spectral response assuming an L-resolution scene model (Strahler, 1986).

Methodology

PCA and multiple linear least square regression models were used to model the relationship between the dependent variable of overall distress rate (ODR) and explanatory variables extracted from the spectral response of the HSR multispectral digital aerial photography. The ultimate goal is to be able to predict the ODR for roadway segments for which ODR ground reference values are unavailable.

Data Acquisition and Preparation

The study area for this research encompasses six counties in northern New Mexico, including Bernalillo, Cibola, Sandoval, Santa Fe, Torrance, and Valencia. These counties are located around the City of Albuquerque and are covered by all of the existing HSR multispectral digital aerial photographs with various spatial resolutions obtained from 2004 to 2012. Within the study area, 50 data collections sites were identified for use in this study. Each data collection site covers the rightmost lane with a length of one tenth of a mile. These sites were selected because they belong to a set of pavement sections regularly evaluated as part of the New Mexico Department of Transportation (NMDOT) pavement evaluation program.

The road segments of these 50 study sites were visually evaluated in reference to the available HSR multispectral digital aerial photographs to ensure they were covered by aerial photographs, and there are no large obstacles (e.g., bridges and overpasses) above them. A geographic information system (GIS) database provides the roadway number, milepost number, and direction for each study site.

Reference pavement surface condition data for the study sites were acquired from records of manual pavement evaluations conducted for NMDOT during the summer of 2009 (Cordova *et al.,* 2009). All of the study sites were constrained to flexible, asphalt pavements. For flexible pavements, the NMDOT evaluates severity and extent of the following seven distresses on a scale of 0 to 3 (0 = Not Present, 1 = Low, 2 = Medium, and 3 = High): (1) Raveling and Weathering; (2) Bleeding; (3) Longitudinal Cracking;(4) Transverse Cracking; (5) Alligator Cracking; (6) Edge Cracking; and (7) Patching. It should be noted that the listed distresses are all horizontal distress, and they do not reflect distresses in elevation such as rutting and shoving. This makes the use of HSR multispectral digital aerial photographs to detect pavement surface overall distress rate (ODR) possible since elevation information cannot be found in a typical aerial photograph (the exception being stereoscopic aerial photographs).

Each study site's ODR can be calculated based on the following equation:

$$\text{ODR} = \sum_{i=1}^{7}(\alpha_i \times \beta_i \times \gamma_i) \quad (1)$$

where i represents each of the seven distresses, α denotes the severity rating, β denotes the extent rating, and γ denotes the weighting factor. The weighting factors for the distresses have been provided by NMDOT and are 3, 2, 12, 12, 25, 3, and 2, respectively, for each of the seven distresses. The calculated ODR for each of the 50 study sites ranges from 0 to 477. The lower the ODR value, the better the pavement condition. The maximum possible value is 504. ODR can be easily converted to Present Serviceability Index (PSI), which is broadly used by various transportation agencies (Bandini *et al.,* 2012). Different agencies can develop and establish their own models to infer the overall pavement surface conditions, no matter what particular metric they are using.

One set of archived and readily available ortho-corrected HSR multispectral digital aerial photographs with a spatial resolution of 6-inches were obtained from the Earth Data Analysis Center (EDAC) at the University of New Mexico. The aerial photographs are natural color digital aerial photography that records energy in the region from 0.4-micrometer to 0.7-micrometer range, and they have three spectral bands which include visible blue (0.4 to 0.5 micrometers), visible green (0.5 to 0.6 micrometers) and visible red (0.6 to 0.7 micrometers) (Jensen, 2007). These images are in 8-bit data format and are the actual digital numbers recorded. In addition, these aerial photographs are routinely (every the other year) collected with the Zeiss/Intergraph Digital Mapping Camera (DMC) System by the Mid-Region Council of Governments (MRCOG) contracted to Bohannan-Huston, Inc.

The aerial photographs were taken in March through April 2010 and were matched with the manually-collected pavement condition data collected in May through August 2009. This was the closest time match between the aerial photographs and the pavement condition data available. According to the Federal Highway Administration, it is approximately a 15-year process for pavement surface condition to drop 50 percent in quality (Lenz, 2011). Because the time elapsed between the pavement condition data collection and aerial photographs collection was less than a year (approximately six months), we assume that no significant change occurred at the study site.

Image Processing

Image Aggregation

Data on actual pavement surface conditions were collected on short sections (0.1-mile [161-meters]) of pavement located at specific mileposts. In order to identify the evaluation zone of each study site on the aerial photographs, a buffer of 0.1-mile was created around each individual study site's milepost in the aerial photographs. After creating the buffers, the evaluation zone of several study sites could not be completely covered by a single 6-inch image, because the aerial photographs were divided into tiles to reduce the storage size. In this case, two or more photographs were needed. When multiple photographs were used for a single milepost, it was necessary to create a mosaic of the aerial photographs. These images were mosaicked based on standard overlay-based algorithm and average blending mode.

Evaluation Polygon Creation

Pavement surface conditions are only evaluated within a portion of the roadway. According to the protocol for manual evaluation employed by NMDOT (Cordova *et al.,* 2009), pavement surface distress data were collected only in the rightmost driving lane and never in passing lanes, turning lanes, or on the shoulder. For two-lane roadways (one driving lane in each direction), data were collected only in the positive direction (north and/or east) from a given milepost to a distance of 0.1-mile. For multi-lane roadways (two or more driving lanes in each direction), data were collected in both the positive and negative directions (north-south and/or east-west) at a given milepost. In the positive direction the pavement evaluation was conducted from a given milepost to a distance of 0.1-mile, while in the negative direction the evaluation was conducted from 0.1-mile prior to the given milepost. This ensured that the pavement sections evaluated at the given milepost were parallel and aligned to each other.

To ensure alignment between the data collection zones, polygons were created to represent the highway zones used in manual evaluation, and from here on referred to as "evaluation polygons." These evaluation polygons were created by heads-up digitizing over the 6-inch resolution aerial photographs following the protocol mentioned above. It should be noted that these manually created polygons only cover the pavement surface, and the polygon creation process does not involve any removal of the non-road surface elements (e.g., vegetation). Therefore, there is no classification involved in the analysis. In addition, there are thousands of pixel cells in

each evaluation polygon and therefore, results are not likely sensitive to omission or commission errors of one or several pixels during the digitizing of evaluation polygons.

When creating the evaluation polygons, six types of features on the ground were excluded since they are considered to be noise. These features are center lines, solid white shoulder stripes, other pavement markings, overpasses, power pole shadows, and vehicles. Figure 1 illustrates the excluded features mentioned above.

Image Degradation

Most counties and municipalities routinely collect HSR multispectral digital aerial photography. The spatial resolution of most of these images is between 6-inch and 1-meter (40-inch). In order to examine how well overall pavement surface distress can be estimated from routinely collected HSR multispectral digital aerial photography, the set of 6-inch aerial photography was degraded to 12-inch (0.3048-meter) and 24-inch (0.6096-meter) aerial photography. This set of 6-inch aerial photography was not degraded to 1-meter because previous research completed by Zhang and Bogus (2014) showed that 1-meter natural color digital aerial photography lacks the spatial resolution to detect overall pavement distress conditions effectively.

Spectral Response Extraction

Only the data within the evaluation polygons are comparable to known ODR rates. Once evaluation polygons were digitized to correspond to the collected reference or actual ODR data, statistics (e.g., mean, median, standard deviation, variety, majority, minority, maximum, minimum, range, and sum) summarizing the pixel values contained within those evaluation polygons were extracted for each resolution.

Multiple Linear Least Squares Regression Analysis

Variables

The dependent variable, or response variable, used in this study is the ODR described in the previous section. ODR was calculated for the field pavement surface distress data collected through manual inspection.

Selecting the most appropriate independent variables from the statistics mentioned in the previous section is necessary for building the regression model. According to Herold (2007), the mean value of the spectral response of the visible wavelengths has a significant negative relationship with ODR. The higher the mean brightness is (higher mean brightness value), the better the pavement surface condition is (lower ODR value). Pavement surface distresses (e.g., cracks) expose deeper layers of the pavement with higher contents of the original asphalt mix, which is then manifested in increased hydrocarbon absorptions features (Herold, 2007). Therefore, degraded pavement surfaces cause less reflectance with increasing hydrocarbon features, while less degraded pavement surfaces get brighter with decreasing hydrocarbon features. Also, shadows induced by cracks decrease brightness.

In this research context, image texture, which is a first order derivative measure of variation in brightness values, may also be a significant variable. Theoretically, the worse the pavement surface condition is, the more heterogeneity of brightness values should be exhibited, due to the introduction of shadows associated with cracks and deformations and exposure of pavement aggregate (i.e., gravels). For example, a very good condition pavement section may have a standard deviation value of 4, while a poor one may have standard deviation value of 100. Pearson's correlation analyses were performed on a variety of texture measures, and it revealed

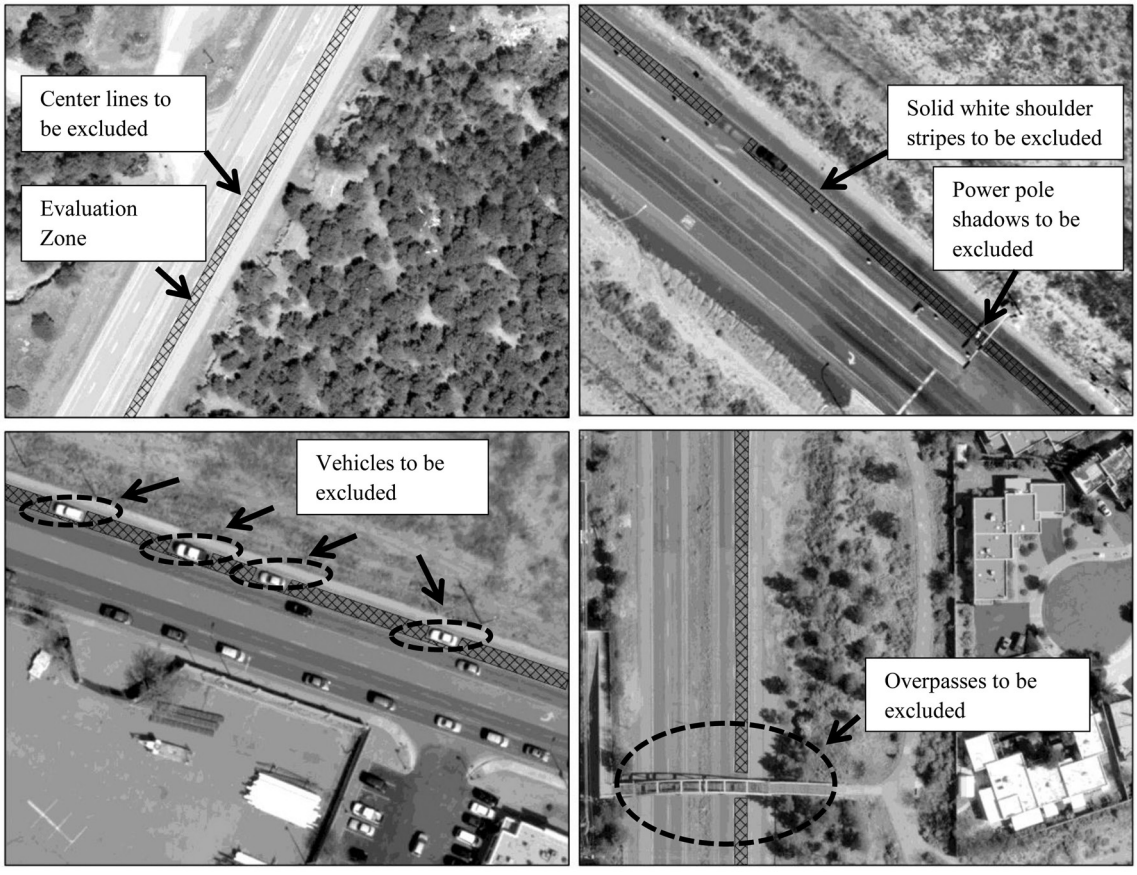

Figure 1. Exclusion of unwanted features on the images.

that other texture measures including range and variety have a strong correlation with standard deviation and therefore, only standard deviation was selected as the texture measure. Table 1 shows the Pearson's correlation results.

For each image dataset, (6-inch, 12-inch, and 24-inch digital aerial photographs), mean and standard deviation values of each band (visible blue, visible green, and visible red) were selected as independent variables, resulting in a total of six variables. Pearson's correlation analyses were performed to examine if there is correlation among these six variables. The results in Table 2 show that in each dataset these six variables have significant correlation with ODR. However, there is also significant correlation among these six variables, which violates the assumption of variable independence by linear least squares regression.

PCA was used on mean and standard deviation values of each band of the three datasets to eliminate the correlation among the six variables (Pearson, 1901). These principal components were used as independent variables for the various linear regression models described below. Table 3 shows the resultant loadings for each principal component obtained from the PCA.

Linear Regression

Various multiple linear least squares regression models were built based on reference pavement surface ODR data and the principal components extracted from the 6-inch, 12-inch, and 24-inch multispectral, digital aerial photographs. The ultimate goal is the identification of the regression model with the highest correlation to predict pavement surface ODR values.

The regression model that uses six principal components obtained from all three visible bands, Model 1 in Table 4, can be expressed as the following equation (Equation 2):

$$\mathrm{ODR}=\beta_0+\beta_1\mathrm{PC}_{A1}+\beta_2\mathrm{PC}_{A2}+\beta_3\mathrm{PC}_{A3}+\beta_4\mathrm{PC}_{A4}+\beta_5\mathrm{PC}_{A5}+\beta_6\mathrm{PC}_{A6} \quad (2)$$

where β_0 represents the intercept parameter, PC_{A1} to PC_{A6} represent the six principal components derived from mean and standard deviation of each band, and β_1 to β_6 represent the corresponding coefficients.

As shown in Table 3, PC_{A1} and PC_{A2} collectively contain more than 99 percent of the information contained in the aerial imagery. In order to test the significance of the rest principal components (PC_{A3} to PC_{A6}), the first two principal components (PC_{A1} and PC_{A2}) were considered as a break point and PC_{A3} to PC_{A6} were removed from the linear regression, resulting in Model 2 (or Equation 3):

$$\mathrm{ODR}=\beta_0+\beta_1\mathrm{PC}_{A1}+\beta_2\mathrm{PC}_{A2} \quad (3)$$

To analyze which spectral band (visible blue, visible green, and visible red) contributes more or is more significant to the prediction of ODR, three linear regression models were created (Models 3 to 5, or Equations 4 to 6) and they are:

$$\mathrm{ODR}=\beta_{B0}+\beta_{B1}PC_{B1}+\beta_{B2}PC_{B2} \quad (4)$$

$$\mathrm{ODR}=\beta_{G0}+\beta_{G1}PC_{G1}+\beta_{G2}PC_{G2} \quad (5)$$

$$\mathrm{ODR}=\beta_{R0}+\beta_{R1}PC_{R1}+\beta_{R2}PC_{R2} \quad (6)$$

PC_{B1} to PC_{B2}, PC_{G1} to PC_{G2}, and PC_{R1} to PC_{R2} represent the two principal components extracted from the mean values and

Table 1. Pearson Correlation Results of Texture Measurement of the 6-Inch, 12-Inch, and 24-Inch Natural Color Digital Aerial Photography.

Dataset	Variables	R1	STD1	V1	R2	STD2	V2	R3	STD3	V3
6-inch	R1	1.0000								
	STD1	0.8738	1.0000							
	V1	0.9790	0.9222	1.0000						
	R2	0.9952	0.8809	0.9816	1.0000					
	STD2	0.8746	0.9977	0.9234	0.8823	1.0000				
	V2	0.9729	0.9267	0.9969	0.9805	0.9300	1.0000			
	R3	0.9869	0.8491	0.9720	0.9876	0.8536	0.9691	1.0000		
	STD3	0.8877	0.9888	0.9362	0.8954	0.9926	0.9417	0.8784	1.0000	
	V3	0.9669	0.8938	0.9884	0.9711	0.8999	0.9891	0.9795	0.9247	1.0000
12-inch	R1	1.0000								
	STD1	0.7680	1.0000							
	V1	0.9001	0.9403	1.0000						
	R2	0.9949	0.7697	0.9007	1.0000					
	STD2	0.7676	0.9972	0.9411	0.7733	1.0000				
	V2	0.8995	0.9342	0.9961	0.9061	0.9395	1.0000			
	R3	0.9814	0.7474	0.8900	0.9898	0.7541	0.8971	1.0000		
	STD3	0.7709	0.9874	0.9466	0.7783	0.9919	0.9450	0.7720	1.0000	
	V3	0.8831	0.9117	0.9861	0.8924	0.9197	0.9901	0.8998	0.9400	1.0000
24-inch	R1	1.0000								
	STD1	0.8041	1.0000							
	V1	0.8915	0.9559	1.0000						
	R2	0.9956	0.7996	0.8826	1.0000					
	STD2	0.8034	0.9962	0.9514	0.8043	1.0000				
	V2	0.8857	0.9518	0.9930	0.8837	0.9535	1.0000			
	R3	0.9742	0.7631	0.8535	0.9845	0.7744	0.8585	1.0000		
	STD3	0.7977	0.9830	0.9451	0.8017	0.9906	0.9495	0.7900	1.0000	
	V3	0.8695	0.9302	0.9780	0.8722	0.9368	0.9843	0.8731	0.9518	1.0000

Note: 1 indicates the visible red band; 2 indicates the visible green band; 3 indicates the visible blue band; R indicates range, STD indicates standard deviation, and V indicates variety.

standard deviation values of the visible blue band, visible green band, and visible red band, respectively. β_{B1} to β_{B2}, β_{G1} to β_{G2}, and β_{R1} to β_{R2} represent the corresponding coefficients. β_{B0}, β_{G0}, and β_{R0} represent the corresponding intercept parameters.

Models 6 and 7 (or Equations 7 to 8) analyze which feature combination (i.e., spectral features [mean values] versus texture features [standard deviation values]) contributes more to the ODR prediction capability, and these two models are:

$$\text{ODR}=\beta_{S0}+\beta_{S1}PC_{S1}+\beta_{S2}PC_{S2}+\beta_{S3}PC_{S3} \quad (7)$$

$$\text{ODR}=\beta_{T0}+\beta_{T1}PC_{T1}+\beta_{T2}PC_{T2}+\beta_{T3}PC_{T3} \quad (8)$$

PC_{S1} to PC_{S3} indicate the three principal components derived from the mean values of each of the three visible bands, and β_{S1} to β_{S3} represent corresponding coefficients. PC_{T1} to PC_{T3} indicate the three principal components extracted from the standard deviation value of each of the three visible bands, and β_{T1} to β_{T3} represent corresponding coefficients. β_{S0} and β_{T0} represent the intercept parameters.

Validation

In order to test the validity and robustness of the method for predicting ODR operationally, we held out 25 of the sites from the identified regression model with the highest certainty described in the previous section. Among the 50 study sites, 25 of them were selected using a random sample stratified by distress rate and used to develop the regression models while the other 25 were used to validate the predicted ODR values by root mean squared error (RMSE), mean absolute error, and standard error.

Results and Discussion

Table 4 shows the linear regression results using all six principal components (PC_{A1} to PC_{A6}) and by using only two principal components (PC_{A1} to PC_{A2}). It revealed that removing PC_{A3} to PC_{A6} decreased the R-squared value and increased the RMSE for all three datasets. It proved that PC_{A3} to PC_{A6} are useful components despite containing less than 1 percent of the original information. This suggests that all six principal components should be used for operational inference of ODR.

Table 4 and Figure 2 show the model fit results (sample size = 50) of the 6-inch, 12-inch, and 24-inch models when using all six principal components. The 6-inch linear regression model is valid at a 95 percent confidence interval (the joint P-value (Prob >F) is less than 0.001). The adjusted R-squared value is 0.9439 and the RMSE is 24.087. This error number is acceptable since the ODR assessed by manual evaluation can exhibit an error of up to 84 or up to 50 percent in terms of variability (Bogus *et al.,* 2010). This implies that natural color aerial photographs with 6-inch spatial resolution can be used to assess and predict overall pavement surface distress rates.

The 12-inch linear regression model is valid at a 95 percent confidence interval (joint P-value (Prob >F) is less than 0.001). The adjusted R-squared value is 0.7958, and the RMSE is 45.843 which is approximately double that of the 6-inch model. This implies that with a higher error, natural color digital aerial photographs with 12-inch resolution can also be used to assess and predict overall pavement surface distress rates. However, 12-inch models still exhibit less error than manual evaluation (45.843 <84).

The 24-inch linear regression model is valid at a 95 percent confidence interval (joint P-value (Prob >F) is less than 0.001). The adjusted R-squared value is 0.6771 and RMSE is 57.645. This implies that natural color aerial photographs with 24-inch resolution can still be used to assess and predict overall pavement surface distress rates, but with the highest error of the resolutions assessed. However, it is still better than the manual evaluation (57.645 <84), and it has the

Table 2. Pearson Correlation Results of the Mean Value and Standard Deviation Value of the 6-Inch, 12-Inch, and 24-Inch Natural Color Digital Aerial Photography

Dataset	Variables	ODR	M1	STD1	M2	STD2	M3	STD3
6-inch	ODR	1.0000						
	M1	-0.9586	1.0000					
	STD1	0.9043	-0.8938	1.0000				
	M2	-0.9512	0.9958	-0.8781	1.0000			
	STD2	0.9075	-0.9016	0.9987	-0.8871	1.0000		
	M3	-0.9333	0.9859	-0.8456	0.9922	-0.8565	1.0000	
	STD3	0.9263	-0.9148	0.9926	-0.9020	0.9953	-0.8764	1.0000
12-inch	ODR	1.0000						
	M1	-0.7337	1.0000					
	STD1	0.8245	-0.6640	1.0000				
	M2	-0.6993	0.9904	-0.6423	1.0000			
	STD2	0.8243	-0.6766	0.9977	-0.6575	1.0000		
	M3	-0.6832	0.9699	-0.6192	0.9881	-0.6390	1.0000	
	STD3	0.8379	-0.6665	0.9892	-0.6518	0.9935	-0.6420	1.0000
24-inch	ODR	1.0000						
	M1	-0.7246	1.0000					
	STD1	0.5457	-0.5072	1.0000				
	M2	-0.7220	0.9863	-0.4397	1.0000			
	STD2	0.5718	-0.5323	0.9977	-0.4669	1.0000		
	M3	-0.7030	0.9455	-0.3497	0.9833	-0.3793	1.0000	
	STD3	0.6022	-0.5236	0.9868	-0.4550	0.9923	-0.3657	1.0000

Note: 1 indicates the visible red band; 2 indicates the visible green band; 3 indicates the visible blue band; M indicates mean; STD indicates standard deviation; and ODR indicates overall distress rate.

TABLE 3. PCA LOADINGS OF THE THREE SETS OF NATURAL COLOR DIGITAL AERIAL PHOTOGRAPHY

Datasets	Input Features	PC	M1	STD1	M2	STD2	M3	STD3	Proportion
6-inch	M1, STD1, M2, STD2, M3, TD3	PC_{A1}	-0.4121	0.4061	-0.4094	0.4083	-0.4022	0.4113	0.9399
		PC_{A2}	0.3313	0.4472	0.3926	0.4162	0.4914	0.3485	0.0568
		PC_{A3}	0.5719	-0.2041	0.2226	-0.0448	-0.6363	0.4182	0.0019
		PC_{A4}	-0.3650	-0.4431	0.0641	-0.2602	0.3184	0.7052	0.0008
		PC_{A5}	0.5072	-0.1174	-0.7890	0.0057	0.3005	0.1269	0.0005
		PC_{A6}	-0.0545	-0.6191	0.0455	0.7684	0.0160	-0.1451	0.0002
	M3, STD3	PC_{B1}	N/A	N/A	N/A	N/A	-0.7071	0.7071	0.9382
		PC_{B2}	N/A	N/A	N/A	N/A	0.7071	0.7071	0.0618
	M2, STD2	PC_{G1}	N/A	N/A	-0.7071	0.7071	N/A	N/A	0.9435
		PC_{G2}	N/A	N/A	0.7071	0.7071	N/A	N/A	0.0565
	M1, STD1	PC_{R1}	-0.7071	0.7071	N/A	N/A	N/A	N/A	0.9469
		PC_{R2}	0.7071	0.7071	N/A	N/A	N/A	N/A	0.0531
	M1, M2, M3	PC_{S1}	0.5772	N/A	0.5784	N/A	0.5319	N/A	0.9942
		PC_{S2}	-0.6196	N/A	-0.1496	N/A	0.7705	N/A	0.0048
		PC_{S3}	0.5319	N/A	-0.8019	N/A	0.2721	N/A	0.0010
	STD1, STD2, STD3	PC_{T1}	N/A	0.5774	N/A	0.5779	N/A	0.5767	0.9970
		PC_{T2}	N/A	-0.5557	N/A	-0.2393	N/A	0.7962	0.0027
		PC_{T3}	N/A	0.5981	N/A	-0.7802	N/A	0.1830	0.0003
12-inch	M1, STD1, M2, STD2, M3, STD3	PC_{A1}	-0.4112	0.4071	-0.4081	0.4114	-0.4021	0.4096	0.8216
		PC_{A2}	0.3849	0.4181	0.4149	0.4005	0.4278	0.4018	0.1707
		PC_{A3}	0.6219	-0.2356	0.0703	-0.0560	-0.6608	0.3361	0.0056
		PC_{A4}	0.4253	0.4615	-0.2630	0.2295	-0.1566	-0.6780	0.0012
		PC_{A5}	0.3392	-0.1144	-0.7630	-0.1575	0.4333	0.2776	0.0006
		PC_{A6}	0.0073	-0.6147	-0.0705	0.7679	0.0797	-0.1449	0.0002
	M3, STD3	PC_{B1}	N/A	N/A	N/A	N/A	-0.7071	0.7071	0.8287
		PC_{B2}	N/A	N/A	N/A	N/A	0.7071	0.7071	0.1713
	M2, STD2	PC_{G1}	N/A	N/A	-0.7071	0.7071	N/A	N/A	0.8210
		PC_{G2}	N/A	N/A	0.7071	0.7071	N/A	N/A	0.1790
	M1, STD1	PC_{R1}	-0.7071	0.7071	N/A	N/A	N/A	N/A	0.8320
		PC_{R2}	0.7071	0.7071	N/A	N/A	N/A	N/A	0.1680
	M1, M2, M3	PC_{S1}	0.5763	N/A	0.5759	N/A	0.5799	N/A	0.9885
		PC_{S2}	-0.6850	N/A	0.7273	N/A	-0.0415	N/A	0.0101
		PC_{S3}	0.4457	N/A	0.3733	N/A	-0.8137	N/A	0.0014
	STD1, STD2, STD3	PC_{T1}	N/A	0.5573	N/A	-0.5776	N/A	0.5771	0.9956
		PC_{T2}	N/A	0.5765	N/A	0.7889	N/A	0.2128	0.0038
		PC_{T3}	N/A	0.5782	N/A	-0.2098	N/A	-0.7885	0.0005
24-inch	M1, STD1, M2, STD2, M3, STD3	PC_{A1}	-0.4248	0.4077	-0.4088	0.4159	-0.3792	0.4117	0.7181
		PC_{A2}	0.3518	0.4129	0.4127	0.3934	0.4701	0.3995	0.2726
		PC_{A3}	0.7108	0.0589	0.0464	0.0942	-0.6929	-0.0122	0.0065
		PC_{A4}	0.0234	-0.5681	0.0526	-0.2084	-0.0630	0.7916	0.0023
		PC_{A5}	0.4357	0.0142	-0.8087	-0.0758	0.3827	0.0615	0.0003
		PC_{A6}	0.0118	-0.5804	-0.0601	0.7837	0.0687	-0.2011	0.0002
	M3, STD3	PC_{B1}	N/A	N/A	N/A	N/A	-0.7071	0.7071	0.7536
		PC_{B2}	N/A	N/A	N/A	N/A	0.7071	0.7071	0.2464
	M2, STD2	PC_{G1}	N/A	N/A	-0.7071	0.7071	N/A	N/A	0.7334
		PC_{G2}	N/A	N/A	0.7071	0.7071	N/A	N/A	0.2666
	M1, STD1	PC_{R1}	-0.7071	0.7071	N/A	N/A	N/A	N/A	0.6829
		PC_{R2}	0.7071	0.7071	N/A	N/A	N/A	N/A	0.3171
	M1, M2, M3	PC_{S1}	0.5745	N/A	0.5825	N/A	0.5751	N/A	0.9812
		PC_{S2}	0.7206	N/A	-0.0266	N/A	-0.6929	N/A	0.0182
		PC_{S3}	0.3883	N/A	-0.8124	N/A	0.4350	N/A	0.0007
	STD1, STD2, STD3	PC_{T1}	N/A	0.5763	N/A	0.5784	N/A	0.5773	0.9949
		PC_{T2}	N/A	0.7890	N/A	-0.2098	N/A	-0.5774	0.0047
		PC_{T3}	N/A	0.2129	N/A	-0.7883	N/A	0.5773	0.0005

Note: PC indicates principal components; $PC_{A1} - PC_{A6}$ indicate the six principal components extracted from the mean and standard deviation values of each of the three visible bands; $PC_{B1} - PC_{B2}$ indicate the two principal components extracted from the mean and standard deviation values of the visible blue band; $PC_{G1} - PC_{G2}$ indicate the two principal components extracted from the mean and standard deviation values of the visible green band; $PC_{R1} - PC_{R2}$ indicate the two principal components extracted from the mean and standard deviation values of the visible red band; $PC_{S1} - PC_{S3}$ indicate the three principal components extracted from the mean values of each of three visible bands; and $PC_{T1} - PC_{T3}$ indicate the three principal components extracted from the standard deviation value of each of the three visible bands.

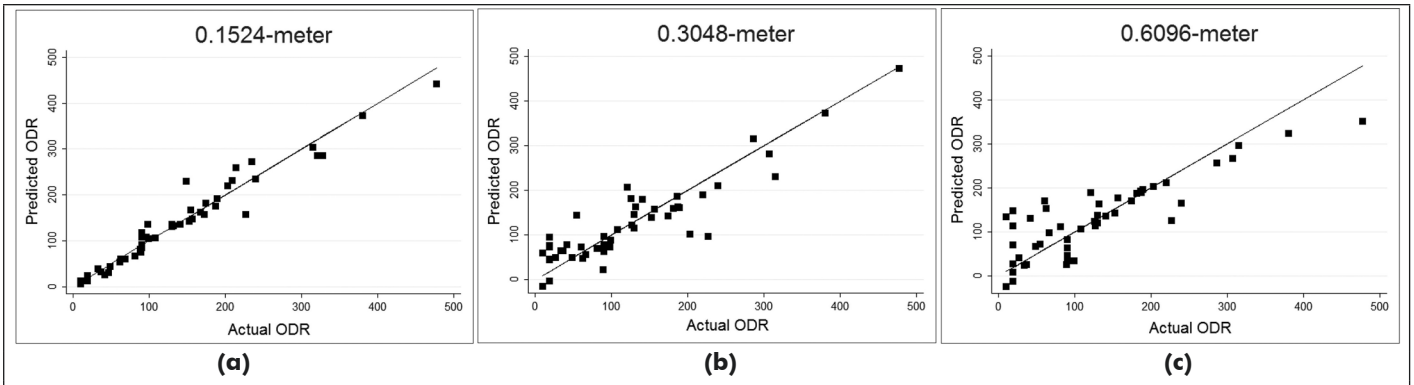

Figure 2. Correlation of predicted ODR versus actual ODR for (a) 6-inch, (b) 12-inch, and (c) 24-inch natural color digital aerial photography

Table 4. Model Fit for Prediction of ODR Values

Dataset (Size: 50)	Model #	Variables	Coefficient	Standard Error	t	P>|t|	R^2	Adjusted R^2	RMSE	Prob > F
6-inch	Model 1	PC_{A1}	41.08	1.45	28.35	<0.001*	0.9507	0.9439	24.087	<0.001*
		PC_{A2}	-13.32	5.89	-2.26	0.029*				
		PC_{A3}	-35.14	32.42	-1.08	0.284				
		PC_{A4}	167.81	48.97	3.43	0.001*				
		PC_{A5}	15.06	64.32	0.23	0.816				
		PC_{A6}	-319.63	112.31	-2.85	0.007*				
		Intercept	135.36	3.41	39.74	<0.001*				
	Model 2	PC_{A1}	41.08	1.69	24.28	<0.001*	0.9266	0.9235	28.123	<0.001*
		PC_{A2}	-13.32	6.88	-1.94	0.059				
		Intercept	135.36	3.98	34.03	<0.001*				
12-inch	Model 1	PC_{A1}	38.68	2.95	13.11	<0.001*	0.8208	0.7958	45.843	<0.001*
		PC_{A2}	14.54	6.47	2.25	0.030*				
		PC_{A3}	-38.51	35.68	-1.08	0.286				
		PC_{A4}	-270.99	76.67	-3.53	0.001*				
		PC_{A5}	-77.86	106.69	-0.73	0.469				
		PC_{A6}	-420.17	175.41	-2.40	0.021*				
		Intercept	125.12	6.48	19.30	<0.001*				
	Model 2	PC_{A1}	38.68	3.41	11.33	<0.001*	0.7378	0.7266	53.045	<0.001*
		PC_{A2}	14.54	7.49	1.94	0.058				
		Intercept	125.12	7.50	16.68	<0.001*				
24-inch	Model 1	PC_{A1}	37.15	3.97	9.36	<0.001*	0.7167	0.6771	57.645	<0.001*
		PC_{A2}	-11.95	6.44	-1.86	0.070				
		PC_{A3}	44.86	41.66	1.08	0.288				
		PC_{A4}	269.66	69.96	3.85	<0.001*				
		PC_{A5}	31.45	186.91	0.17	0.867				
		PC_{A6}	-337.52	266.20	-1.27	0.212				
		Intercept	125.12	8.15	15.35	<0.001*				
	Model 2	PC_{A1}	37.15	4.51	8.24	<0.001*	0.6004	0.5834	65.484	<0.001*
		PC_{A2}	-11.95	7.31	-1.63	0.109				
		Intercept	125.12	9.26	13.51	<0.001*				

Note: PC_{A1} to PC_{A6} indicate the six principal components extracted from the mean and standard deviation values of each of the three visible bands; RMSE indicates root mean squared error; and * indicates the independent variable is significant at p = 0.05 level.

Table 5. Test of a Variety of Options to Infer Overall Distress Rates

Dataset (Size: 50)	Model #	Variables	Coefficient	Standard Error	t	P>|t|	R^2	Adjusted R^2	RMSE	Prob > F
6-inch	Model 3	PC_{B1}	71.24	3.03	23.52	<0.001*	0.9217	0.9184	29.041	<0.001*
		PC_{B2}	-4.09	11.80	-0.35	0.731				
		Intercept	135.36	4.11	32.96	<0.001*				
	Model 4	PC_{G1}	70.80	2.98	23.77	<0.001*	0.9239	0.9206	28.643	<0.001*
		PC_{G2}	-27.78	12.18	-2.28	0.027*				
		Intercept	135.36	4.05	33.42	<0.001*				
	Model 5	PC_{R1}	70.71	2.85	24.82	<0.001*	0.9301	0.9271	27.442	<0.001*
		PC_{R2}	-36.70	12.03	-3.05	0.004*				
		Intercept	135.36	3.88	34.88	<0.001*				
	Model 6	PC_{S1}	-55.95	2.39	-23.38	<0.001*	0.9240	0.9190	28.924	<0.001*
		PC_{S2}	120.37	34.35	3.50	<0.001*				
		PC_{S3}	-34.09	76.27	-0.45	0.657				
		Intercept	135.36	4.09	33.09	<0.001*				
	Model 7	PC_{T1}	53.73	2.99	17.94	<0.001*	0.8806	0.8728	36.252	<0.001*
		PC_{T2}	226.37	58.01	3.90	<0.001*				
		PC_{T3}	241.83	165.58	1.46	0.151				
		Intercept	135.36	5.13	26.40	<0.001*				
12-inch	Model 3	PC_{B1}	67.17	5.83	11.52	<0.001*	0.7231	0.7113	54.510	<0.001*
		PC_{B2}	19.39	12.97	1.49	0.142				
		Intercept	125.12	7.44	16.81	<0.001*				
	Model 4	PC_{G1}	66.45	5.91	11.24	<0.001*	0.7379	0.7268	53.030	<0.001*
		PC_{G2}	31.01	12.66	2.45	0.018*				
		Intercept	125.12	7.50	16.68	<0.001*				
	Model 5	PC_{R1}	65.94	6.05	10.90	<0.001*	0.7418	0.7308	52.638	<0.001*
		PC_{R2}	26.19	13.31	1.97	0.055				
		Intercept	125.12	7.71	16.23	<0.001*				
	Model 6	PC_{S1}	48.76	4.64	10.52	<0.001*	0.7129	0.6942	56.103	<0.001*
		PC_{S2}	104.05	74.77	1.39	0.171				
		PC_{S3}	262.22	199.84	1.31	0.196				
		Intercept	125.12	7.93	15.77	<0.001*				
	Model 7	PC_{T1}	-41.79	5.61	-7.45	<0.001*	0.5832	0.5560	67.602	<0.001*
		PC_{T2}	116.54	55.58	2.10	0.042*				
		PC_{T3}	-311.73	148.31	-2.10	0.041*				
		Intercept	125.12	9.56	13.09	<0.001*				
24-inch	Model 3	PC_{B1}	68.56	7.68	8.92	<0.001*	0.5677	0.5494	68.105	<0.001*
		PC_{B2}	-11.40	11.28	-1.01	0.066				
		Intercept	125.12	8.89	14.07	<0.001*				
	Model 4	PC_{G1}	63.27	7.81	8.10	<0.001*	0.5917	0.5743	66.190	<0.001*
		PC_{G2}	-20.21	12.95	-1.56	0.125				
		Intercept	125.12	9.36	13.37	<0.001*				
	Model 5	PC_{R1}	68.59	7.68	8.92	<0.001*	0.6317	0.6160	62.865	<0.001*
		PC_{R2}	-11.40	11.28	-1.01	0.317				
		Intercept	125.12	8.89	14.07	<0.001*				
	Model 6	PC_{S1}	-42.78	5.99	-7.15	<0.001*	0.5285	0.4978	71.898	<0.001*
		PC_{S2}	27.26	43.98	0.62	0.539				
		PC_{S3}	-82.25	231.18	-0.36	0.724				
		Intercept	125.12	10.17	12.31	<0.001*				
	Model 7	PC_{T1}	33.75	6.21	5.43	<0.001*	0.4856	0.4521	75.096	<0.001*
		PC_{T2}	290.84	90.70	3.21	0.002*				
		PC_{T3}	-540.37	284.34	-1.90	0.064				
		Intercept	125.12	10.62	11.78	<0.001*				

Note: $PC_{B1} - PC_{B2}$ indicate the two principal components extracted from the mean and standard deviation values of the visible blue band; $PC_{G1} - PC_{G2}$ indicate the two principal components extracted from the mean and standard deviation values of the visible green band; $PC_{R1} - PC_{R2}$ indicate the two principal components extracted from the mean and standard deviation values of the visible red band; $PC_{S1} - PC_{S3}$ indicate the three principal components extracted from the mean values of each of the three visible bands; $PC_{T1} - PC_{T9}$ indicate the three principal components extracted from the standard deviation value of each of the three visible bands; and * indicates the independent variable is significant at p = 0.05 level.

Table 6. Model Validation for Prediction of ODR Values

Dataset (Size: 25)	Variables	Coefficient	Standard Error	t	P>|t|	R^2	Adjusted R^2	RMSE	Prob > F
6-inch	PC_{A1}	46.03	3.22	14.29	<0.001*	0.9232	0.8976	37.206	<0.001*
	PC_{A2}	-13.17	11.74	-1.12	0.277				
	PC_{A3}	-102.89	61.00	-1.69	0.109				
	PC_{A4}	264.22	129.98	2.03	0.057				
	PC_{A5}	-43.32	152.78	-0.28	0.780				
	PC_{A6}	-539.59	272.10	-1.98	0.063				
	Intercept	137.28	7.44	18.45	<0.001*				
12-inch	PC_{A1}	45.33	5.12	8.85	<0.001*	0.8178	0.7571	57.309	<0.001*
	PC_{A2}	-4.55	13.65	-0.33	0.743				
	PC_{A3}	42.88	59.73	0.72	0.482				
	PC_{A4}	-175.53	143.74	-1.22	0.238				
	PC_{A5}	50.69	241.64	0.21	0.836				
	PC_{A6}	187.02	335.35	0.56	0.584				
	Intercept	137.28	11.46	11.98	<0.001*				
24-inch	PC_{A1}	33.06	7.73	4.28	<0.001*	0.7166	0.6222	71.476	<0.001*
	PC_{A2}	-42.78	9.45	-4.53	<0.001*				
	PC_{A3}	125.42	76.79	1.63	0.120				
	PC_{A4}	-231.38	118.32	-1.96	0.066				
	PC_{A5}	-88.60	300.07	-0.30	0.771				
	PC_{A6}	194.58	486.38	0.40	0.694				
	Intercept	137.28	14.30	9.60	<0.001*				

Note: PC_{A1} and PC_{A6} indicate the six principal components extracted from the mean and standard deviation values of each of the three visible bands; RMSE indicates root mean squared error; and * indicates the independent variable is significant at p = 0.05 level.

advantage of lower cost when compared to higher spatial resolution datasets.

In order to investigate the principles of using HSR multispectral digital aerial photography to infer ODR, we performed various linear regression models (Models 3 to 7) by using only one visible band and by using only spectral features (mean values) or texture features (standard deviation values). The results were summarized in Table 5. The results revealed that the visible red band best predicts ODR at all spatial resolutions (e.g., 6-inch dataset R^2 >93% and RMSE <28), while visible blue band predicts ODR at the lowest certainty. Table 5 also revealed that when compared to texture features, spectral features predict ODR at a higher certainty (e.g., 6-inch dataset R^2 >92% and RMSE <29).

Results revealed that the regression model that uses all six principal components exhibited the best capability to predict ODR. Therefore, this model was selected for validation. Table 6 shows the results of the 6-inch, 12-inch, and 24-inch regression models when using only half of the study sites for calibration (sample size =25). It shows that the R-squared value is decreased while the RMSE is increased for all three models, but not substantially. All three models are still valid at a 95 percent confidence interval (joint P-value (Prob >F) is less than 0.001).

The other 25 study sites were used to independently validate predicted (model-generated) ODR values versus actual (ground reference) ODR values, the RMSE, mean absolute error, and standard error of which are shown in Table 7. Not surprisingly, the RMSE for each model is higher when validated using holdout samples and predicted using the smaller sample size of 25 to develop the model, but not substantially. In addition, the mean absolute error and standard error are increased when the resolution becomes coarser, but all are less than an error of 84 that manual evaluation can exhibit.

Table 7. Error Summary for Predicted ODR

Dataset (Size: 25)	RMSE	Mean Absolute Error	Standard Error
6-inch	42.8826	35.0000	5.0577
12-inch	63.1958	43.7600	9.3070
24-inch	72.5551	66.2400	12.0770

Validation results, consistent with model fits, show that the 6-inch aerial photography results in the lowest error when compared to manual evaluation results, whether measured by RMSE, mean absolute error, or standard error. Therefore, we conclude that ODR can be most effectively predicted by the 6-inch aerial photography. While none of the models can be used to detect detailed distress (e.g., cracks) or vertical distress (e.g., rutting), all models indicate potential for the direct estimation of ODR with less error than manual approaches.

One limitation of the proposed method is that it cannot be used for high traffic volume sections. This is because vehicles are considered as unwanted features on the pavement. Too many vehicles present in the images could reduce the area of pavement observed to such a degree that distress cannot be accurately evaluated. This proposed method also must use reference pavement surface distress rates (collected either through manual evaluation or automatic evaluation) to develop initial model calibrations.

Conclusions

Routine evaluation of pavement surface condition is a challenge to all transportation agencies. In the real world, it is impossible to get exhaustive condition data for all pavement surfaces. Current methods for pavement surface distress

evaluation are labor-intensive, time-consuming, and expensive. To overcome these limitations, we present a novel approach for overall pavement surface condition evaluation through the analysis of routinely-acquired and publically-available HSR multispectral digital aerial photographs. These images are already paid for through a variety of means, permitting a dramatic reduction in the cost of intensive survey through manual or automated samples, making it extremely practical and immediately implementable across all regions without tree cover. Our results have shown that natural color aerial photographs of 6-inch spatial resolution can be used to evaluate the overall pavement distress conditions with a high degree of certainty (R^2 >95%). At a lesser degree of certainty, 12-inch and 24-inch natural color aerial photographs can also be used to detect overall pavement conditions. When considering the associated cost, the lower resolution aerial photographs can be potentially applied to evaluate overall pavement surface distress for rapid, high-level information checks. Our results also have shown that visible red band or spectral features alone can be used to estimate the overall pavement conditions with a high degree of certainty (R^2 >92%).

The proposed method of detecting pavement surface distress conditions by analyzing HSR multispectral, digital aerial photography could be used as a predictor of overall distress conditions in situations where field inspectors cannot evaluate except with considerable labor (e.g., sections in remote areas). It is not likely that the proposed method will completely replace field pavement surface inspection due to its lack of crack-level detailed pavement surface information and the necessity of using field pavement surface inspection results as reference data to develop the regression models. However, the spectral response in HSR multispectral digital aerial photography presents additional information not considered in field inspection and could be used to predict the overall pavement surface conditions in un-sampled areas based on a dramatically reduced number of intensive survey sites. Therefore, it can reduce the amount of work, time, and money associated with pavement surface evaluation. Operationally this proposed approach could be readily implemented as a service internally by transportation agencies such as NMDOT or implemented through consulting firms. Eventually this proposed method could be automated through software development. Such software would only require users to insert the pavement surface distress rates of a limited number of manual survey sites, add associated HSR multispectral digital aerial photography, and upload the evaluation polygon, while the computing-intensive processes such as eliminating unwanted features is fully automated.

Acknowledgments

We would like to express our greatest gratitude to New Mexico Department of Transportation (NMDOT) and Earth Data Analysis Center (EDAC) at the University of New Mexico (UNM). Without their enormous support, it would not have been possible to complete this research. Thanks also go to the PE&RS journal editor and anonymous reviewers for their valuable comments to improve this paper.

References

Adarkwa, O.A., and N. Attoh-Okine, 2013. Pavement crack classification based on Tensor Factorization, *Journal of Construction and Building Materials*, 48:853–857.

Bandini, P., S.M. Bogus, K. Montoya, H. Pham, and G.C. Migliaccio, 2012. *Improving NMDOT's Pavement Distress Survey Methodology and Developing Correlations between FHWA's HPMS Distress Data and PMS Data*, New Mexico Department of Transportation Research Bureau Report NM10MNT-01.

Bogus, S.M., J. Song, R. Waggerman, and L. Lenke, 2010. Rank correlation method for evaluating manual pavement distress data variability, *Journal Infrastructure Systems*, 16(1):66–72.

Chen, S., C. Rice, C. Boyle, and E. Hauser, 2011. Small-format aerial photography for highway-bridge monitoring, *Journal of Performance of Constructed Facilities*, 25(2):105–112.

Cheng, H.D., X. Jiang, J. Li, and C. Glazier, 1999. Automated real-time pavement distress Analysis, *Transportation Research Record*, 1655:55–64.

Cordova, A.A., S.M. Bogus, G.C. Migliaccio, and L.R. Lenke, 2009. *2009 Pavement Evaluation Report: Northern New Mexico*, Report prepared by University of New Mexico for New Mexico Department of Transportation State Maintenance Bureau SB-2.

Coudray, N., A. Karathanou, and S. Chambon, 2010. Multi-resolution approach for fine structure extraction - Application and validation on road Images, *Proceedings of the 5th International Conference on Computer Vision Theory and Applications*, 17-21 May, Angers, France, pp. 142–147.

Curphey, D.R., D.K. Fronek, and J.H. Wilson, 1985. Highway pavement surface remote sensing using video image processing, *Proceedings of the ASCE Spring Convention*, *Convention*, 29 April-02 May 1986, Denver, Colorado, unpaginated CD-ROM.

Gavilan, M., D. Balcones, O. Marcos, D.F. Llorca, M.A. Sotelo, I. Parra, M. Ocana, E. Aliseda, P. Yarza, and A. Amirola, 2011. Adaptive road crack detection system by pavement classification, *Journal of Sensors*, 11:9628–9657.

Gramling, W.L., 1994. *Current Practices in Determining Pavement Condition: NCHRP Synthesis of Highway Practice No. 203*, Transportation Research Board.

Georgopoulos, A., A. Loizos, and A. Flouda, 1995. Digital image processing as a tool for pavement distress evaluation, *ISPRS Journal of Photogrammetry and Remote Sensing*, 50(1):23–33.

Haas, C., H. Shen, W.A. Phang, and R. Haas, 1985. An expert system for automation of pavement condition inventory data, *Proceedings of the 1st North American Pavement Management Conference,* 28-31 March 1985, Toronto, Canada, pp.4.46–4.57.

Haas, R., W.R. Hudson, and J. Zaniewski, 1994. *Modern Pavement Management*, Krieger, Malamar, Florida, 36 p.

Herold, M., 2007. *Remote Sensing of Impervious Surfaces*, CRC Press, Boca Raton, Florida, 242 p.

Huang,Y., and B. Xu, 2006. Automatic inspection of pavement cracking distress, *Journal of Electronic Imaging*, 15(1):0130171–0130176.

Hudson, W.R., G.E. Elkins, W. Uddin, and K.T. Reilley, 1987. *Improved Methods and Equipment to Conduct Pavement Distress Surveys*, Report FHWA-TS-87-213 prepared by ARE, Inc. for the Federal Highway Administration.

Hudson, W.R., and W. Uddin, 1987. Future pavement evaluation technologies: Prospects and opportunities, *Proceedings of the 2nd North American Pavement Management Conference*, 02-06 November, Toronto, Canada, pp. 3.233–3.258.

Jensen, J.R., 2007. *Remote Sensing of the Environment: An Earth Resource Perspective*, Second edition, Prentice Hall, Upper Saddle River, New Jersey, 592 p.

Koch, C., and I. Brilakis, 2011. Pothole detection in asphalt pavement images, *Journal of Advanced Engineering Informatics*, 25(3):507–515

Lee, H.D., and J.J. Kim, 2005. Development of a crack type index, *Transportation Research Record*, 1940:99–109.

Lenz, R.W., 2011. *Pavement Design Guide - Flexible Pavement Design System (FPS) 19: User's Manual*, Texas Department of Transportation.

Mahler, D.S., Z.B. Kharoufa, E.K. Wong, and L.G. Shaw, 1991. Pavement distress analysis using image processing techniques, *International Journal of Microcomputers in Civil Engineering*, 6(1):1–14.

McGhee, K.H., 2004. *Automated Pavement Distress Collection Techniques – A Synthesis of Highway Practice*, National Cooperative Highway Research Program, Transportation Research Board.

McMaster, H.M., and A.R. Legault, 1952. *Pavement Condition Surveys by Means of Aerial Photography*, University of Nebraska Press, Lincoln, Nebraska.

Nguyen, T.S., M. Avila, S. Begot, F. Duculty, and J.C. Bardet, 2009. Automatic detection and classification of defect on road Pavement using anisotropy measure, *Proceedings of the 17th European Signal Processing Conference*, 24-28 August, Glasgow, Scotland, pp.617–621.

Oliveira, H., and P.L. Correia, 2008. Identifying and retrieving distress images from road pavement surveys, *Proceedings of the 1st Workshop on Multimedia Information Retrieval: New Trends and Challenges, International Conference on Image Processing*, 12-15 October, San Diego, California, pp.57–60.

Pearson, K., 1901. On lines and planes of closest fit to systems of points in space, *Philosophical Magazine*, 2(11):559–572.

Prakash, A., B.N. Sharma, and T.J. Kazmierowski, 1994. Investigation into observational variations in pavement condition survey, *Proceedings of the 3rd International Conference on Managing Pavements*, Transportation Research Board, 22-26 May, Washington, D.C., pp. 290–301.

Pynn, J., A. Wright, and R. Lodge, 1999. Automatic identification of cracks in road surfaces, *Proceedings of the 7th International Conference on Image Processing and Its Applications*, IEEE, 13-15 July, Manchester, UK, pp. 671–675.

Stoeckeler, E G., 1968. *Use of Color Aerial Photography for Pavement Evaluation Studies in Maine*, Maine State Highway Commission, Material and Research Division.

Stoeckeler, E.G., 1970. Use of aerial color photography for pavement evaluation studies, *Highway Research Record*, 319:40–57.

Strahler, A.H., C.E. Woodcock, and J.A. Smith, 1986. On the nature of models in remote sensing, *Remote Sensing of Environment*, 20(2):121–139.

Uddin, W., W.R. Hudson, and G.E. Elkins, 1987. *Evaluation of Equipment for Measuring Voids under Pavements*, Draft Report FH67/3 prepared by ARE, Inc. for the Federal Highway Administration.

Wang, K.C.P., 2000. Designs and implementations of automated systems for pavement surface distress survey, *Journal of Infrastructure Systems*, 6(1):24–32.

Wang, K.C.P., and X. Li, 1999. Use of digital cameras for pavement surface distress Survey, *Transportation Research Record,* 1675:91–97.

Wright, P., 2014. Missouri state wide imagery program, Missouri GIS Advisory Council's Data Development Committee, URL: *http://www.flymoimagery.com/*, Office of Geospatial Information, Jefferson City, Missouri, (last date accessed: 22 July 2015).

Zhang, S., and S.M. Bogus, 2014. Use of low-cost remote sensing for infrastructure management, *Proceedings of the 2014 Construction Research Congress*, 19-21 May, Atlanta, Georgia, pp. 1299–1308.

Zhou, J., P. Huang, and F.P., Chiang, 2006. Wavelet-based pavement distress detection and evaluation, *Optical Engineering*, 45(2):027007-1–027007-10.

(Received 11 February 2015; accepted 24 March 2015; final version 29 March 2015)